Formation of NH_3-Xe compound at the extreme condition of planetary interiors

Pan Zhang,[1] Jingming Shi,[1,*] Wenwen Cui,[1] Cailong Liu,[2] Shicong Ding,[1] Kang Yang,[1] Jian Hao,[1] and Yinwei Li[1,2,†]

[1]*Laboratory of Quantum Functional Materials Design and Application, School of Physics and Electronic Engineering, Jiangsu Normal University, Xuzhou 221116, China*

[2]*Shandong Key Laboratory of Optical Communication Science and Technology, School of Physical Science & Information Technology of Liaocheng University, Liaocheng 252059, China*

(Received 19 February 2022; revised 28 May 2022; accepted 2 June 2022; published 21 June 2022)

Noble gas elements have been illustrated to exhibit chemical activity to form unconventional compounds at high pressure. In this paper, we report combined structure prediction and first-principles calculations to propose an unexpected stoichiometry of $(NH_3)_2Xe$ that becomes energetically stable >11 GPa. Here, NH_3 in the compound remains in its molecular form up to at least 300 GPa, indicating that the incorporation of Xe could suppress the ionization of NH_3. *Ab initio* molecular dynamics simulations reveal that $(NH_3)_2Xe$ transforms from a solid to a superionic, and finally to a fluid as the temperature increases. The superionic phase remains stable in the pressure and temperature region that covers the extreme conditions of the layer outside the core of planets such as Uranus, Neptune, Venus, and Earth. This suggests that $(NH_3)_2Xe$ is a possible constituent of planetary interiors. The current results provide theoretical evidence that Xe could be trapped inside planets during their evolution and could help to update models of planetary interiors.

DOI: 10.1103/PhysRevB.105.214109

I. INTRODUCTION

The noble gases are generally unreactive due to their stable closed-shell electronic configuration. However, high pressure can reorder the energy of the outer atomic orbital and modify the chemical oxidation state to induce unexpected stoichiometries. Authors of recent studies have identified chemical reactivity in He and Xe at high pressure and the formation of several unexpected compounds that are inaccessible at ambient conditions. Various van der Waals compounds including H_2O-He [1,2], Na_2He [3], HeN_4 [4], NH_3-He [5,6], O-Xe [7–14], H-Xe [15,16], and H_2O-Xe [17] have been proposed or confirmed to be energetically stable at high pressure. These studies not only expand the chemistry of noble gas compounds but also provide a theoretical guide for further searches of compounds of noble gases at extreme conditions.

The noble gases, especially He and Xe, are abundant in the atmospheres of icy planets such as [18–21], Earth [22], Jupiter, and Venus [23–26], and they are generally not considered to remain in planetary interiors during their evolution owing to their light atomic mass and chemical inertness [27]. Authors of many theoretical studies have considered whether He or Xe could form compounds with components such as NH_3, CH_4, and H_2O at high pressures and high temperatures (HPHT) corresponding to the conditions inside planets [7–16,28–30]. Recent theoretical works have illustrated that He could be trapped in planetary interiors in the form of stable compounds (H_2O-He [1,2], NH_3-He [5,6], and CH_4-He [31]); such findings contribute to the understanding and modeling of the formation and evolution of planets. Many constituents of Earth have been proposed to react with Xe to form stable compounds at extreme conditions, e.g., Xe-Fe/Ni [32], Xe-FeO_2 [33], and Xe-SiO_2 [34]. Authors of these studies provide essential information for explaining the missing Xe paradox [35–37]. Additional experimenters have found that Xe can react with water ice at 50 GPa and 1500 K to form $Xe_4O_{12}H_{12}$, which could possibly exist in the layer outside the core of giant planets such as Uranus and Neptune [17]. However, these results do not fully explain the formation, evolution, and interior models of planets. Therefore, exploring the internal components of planets is an important issue in high-pressure condensed matter physics and geoscience.

In this paper, we report combined structure predictions and first-principles calculations and the surprising finding that Xe could react with NH_3 at pressures >11 GPa to form an unconventional compound $(NH_3)_2Xe$, which transforms into a superionic phase at high temperature. Interestingly, the stable pressure and temperature regions of superionic $(NH_3)_2Xe$ cover the extreme conditions corresponding to the interiors of planets such as Uranus, Neptune [38], Jupiter, and Venus [25,26]. These results reveal that the predicted compound might be a constituent of the layer outside the core of these planets. The current results aid the understanding of the interior models of these planets.

II. METHODS

The structural prediction for $(NH_3)_xXe_y$ ($x = 1$–3, $y = 1$–3) systems at 50, 100, 200, and 300 GPa is by CALYPSO [39–41] based on a global minimization of potential energy surfaces in conjunction with *ab initio* total energy calculations. The CALYPSO prediction method has successfully predicted various

*jingmingshi@jsnu.edu.cn
†yinwei_li@jsnu.edu.cn

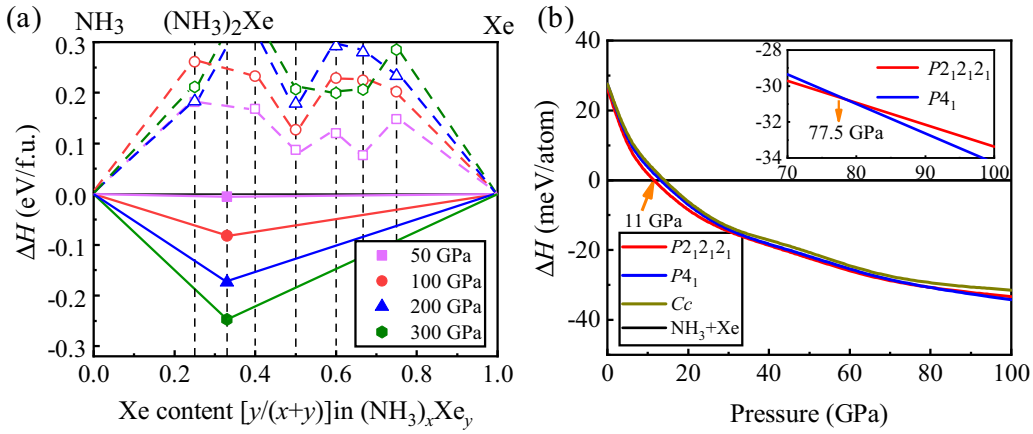

FIG. 1. (a) Convex hull of formation enthalpies (ΔH) of the NH_3-Xe system with respect to decomposition into solid NH_3 and Xe at selected pressures, defined as $\Delta H = \{H[(NH_3)_xXe_y] - xH(NH_3) - yH(Xe)\}/(x+y)$. (b) Calculated formation enthalpies of the $P2_12_12_1$ and $P4_1$ structures as a function of pressure. The inset magnifies the crossover region corresponding to the phase transformation from the $P2_12_12_1$ to the $P4_1$ structure. The calculations adopt the $P2_13$ structure at 0–10 GPa, $P2_12_12_1$ at 10–90 GPa, and $Pma2$ at 90–300 GPa for NH_3 [62,63] and the $P6_3/mmc$ and $Fm\bar{3}m$ structures for Xe at 0–300 GPa [64].

systems under high pressure [42–51]. We performed structural searches on each composition with maximum simulation cells up to 4 f.u. Structural relaxations are done by using density functional theory, as implemented in the Vienna *Ab initio* Simulation Package (VASP) [52,53], adopting the Perdew-Burke-Ernzerhof exchange-correlation functional under the generalized gradient approximation [54,55]. All-electron projector augmented wave pseudopotentials with $2s^22p^3$, $1s^1$, and $5s^25p^6$ valence configurations were chosen for N, H, and Xe atoms, respectively [56]. A plane-wave cutoff energy of 1000 eV and k-point mesh of $2\pi \times 0.03$ Å^{-1} ensure convergences of total energy and forces better than 1 meV/atom and 1 meV/Å, respectively. The phonon dispersions of the predicted structures were calculated using a finite displacement method, as implemented in the PHONOPY code. *Ab initio* molecular dynamics (AIMD) simulations explore the atomic dynamical properties of $(NH_3)_2Xe$ at a series of selected pressures and temperatures. A supercell containing 144 atoms is used, and the Brillouin zone is sampled at the Γ point. Each simulation, running for 10 000 time steps of 1 fs, uses the NVT ensemble applying a Nosé-Hoover thermostat [57] with SMASS = 2. We also performed the AIMD calculations by setting SMASS = 1 to check the accuracy, as shown in Fig. S1 in the Supplemental Material (SM) [58], and ensuring that the value of SMASS does not affect the final result. After thermalization for 1 ps, we analyzed the exact data and calculated the mean square displacement to clarify the atomic thermal character. Crystal structures and electron localization functions (ELFs) are plotted using VESTA software [59]. All calculations for the formation enthalpies and enthalpy differences are considered the zero-point vibration energies and van der Waals corrections with the DFT-D3 functional [60,61].

III. RESULTS AND DISCUSSION

To determine the thermodynamic stability of the NH_3-Xe system, the convex hull depicts calculated formation enthalpies for each composition at different pressures. Figure 1(a) shows that a compound with a 2:1 ratio of NH_3 and Xe possesses a negative formation enthalpy at 50 GPa, which becomes more negative as pressure increases to 100, 200, and 300 GPa. Figure 1(b) indicates that the onset pressure of $(NH_3)_2Xe$ becoming stable with respect to a mixture of NH_3 and Xe is as low as 11 GPa. At low pressure, $(NH_3)_2Xe$ adopts a $P2_12_12_1$ symmetry and is composed of isolated Xe atoms and ammonia molecules. The ammonia molecules align in two crossing planes forming face-sharing rhombic prisms parallel to the a axis (dotted lines), and the isolated Xe atoms are located inside these prisms, as shown in Fig. 2(a). At 11 GPa, the N-H bond lengths in $(NH_3)_2Xe$ are between 1.023 and 1.029 Å, which is very close to that (1.022 to 1.03 Å) in pure crystalline NH_3 [62], whereas the shortest N-Xe distance is ∼3.4 Å. With increasing pressure, the $P2_12_12_1$ structure becomes energetically unstable and transforms into the $P4_1$ phase at 77.5 GPa via rearrangement of the NH_3 molecules. The $P4_1$ structure is still composed of NH_3 molecules aligned in two crossing planes and isolated Xe located inside the rhombic prisms, as shown in Fig. 2(b). The only difference between the two structures is the position and orientation of the NH_3 molecules on the crossing planes. Given the similar arrangements of NH_3 in these structural configurations, their energies are very close (<5 meV/atom) across the whole range of pressures at which they are stable. The N-H bond length in the $P4_1$ structure is ∼1.01 Å at 80 GPa. To examine whether the $P2_12_12_1$ and $P4_1$ structures have the same Xe-N sublattices, we have checked the two structures after the removal of H atoms. In fact, although the two Xe-N sublattices are geometrically similar, they have different symmetries with slightly different Xe-N distances and N-Xe-N angles (Fig. S2 in the SM [58]). Therefore, the $P2_12_12_1$ and $P4_1$ structures are two different crystal phases of $(NH_3)_2Xe$ at high pressure. In addition, we also calculated the energy barriers corresponding to the different rotation states based on the $P2_12_12_1$ structure at the phase transition pressure of 80 GPa (Fig. S3 in the SM [58]), and the maximum energy barrier of 40 meV/atom is much higher than that (∼10 meV/atom) in the orientationally disordered hexagonal close-packed phase of solid H_2 [65]. Therefore, we deduced that NH_3 cannot rotate freely in

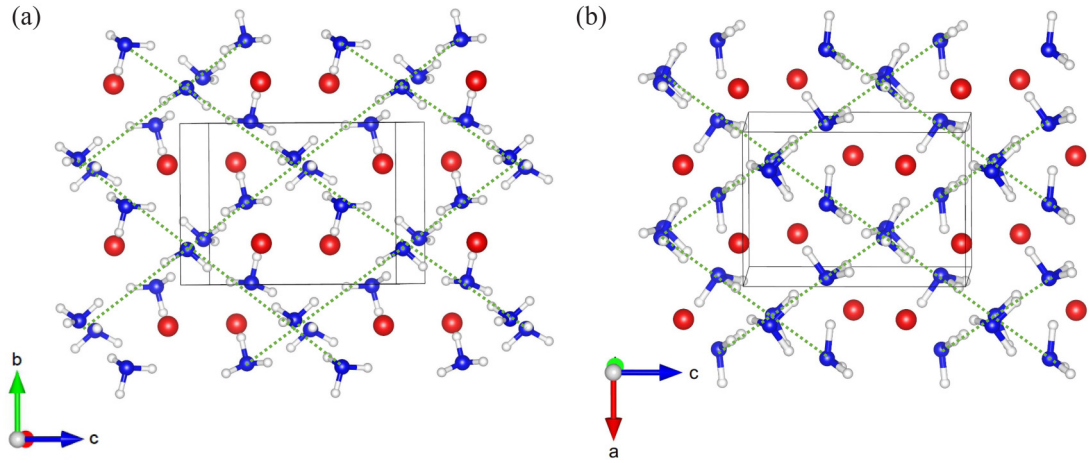

FIG. 2. Structures predicted for $(NH_3)_2Xe$: (a) $P2_12_12_1$ at 11 GPa and (b) $P4_1$ at 80 GPa. Blue, white, and red atoms represent N, H, and Xe atoms, respectively. The green dotted lines represent the planes on which the ammonia molecules are aligned.

$(NH_3)_2Xe$. In addition, there is an energetically competitive phase related to the $P4_1$ structure; it possesses Cc symmetry, as shown in Fig. S4 in the SM [58]. The enthalpy of the Cc phase is only ∼1.5 meV/atom higher than that of the $P4_1$ phase across the whole pressure range (Fig. S5(a) in the SM [58]), suggesting that this competitive structure could be a potentially synthesizable metastable phase of $(NH_3)_2Xe$. We have also compared the energy differences of two structures by performing structure optimization using the SCAN functional [66,67]. As compared in Fig. S5(b) in the SM [58], the use of the new functional does not change the relative stability of the two structures; the only difference is that the energy difference increases to a maximal 4 meV/atom. Table S1 in the SM [58] summarizes the structural parameters of all predicted phases.

The ELFs of $(NH_3)_2Xe$ are calculated at 11, 80, 200, and 300 GPa to determine its chemical bonding characteristics (Fig. S6 in the SM [58]). The ELFs show electrons localized between the N and H atoms, revealing typical covalent bonding in the NH_3 molecules. However, the absence of electron localization between Xe and NH_3 precludes covalent interactions between them. The NH_3 molecules in $(NH_3)_2Xe$ are preserved at least up to 300 GPa, which is different from the ionic behavior of NH_3 and NH_3-He compounds composed of $(NH_4)^+$ and $(NH_2)^-$ at >100 GPa [5,6,62]. This indicates that the incorporation of Xe could inhibit the ionization of NH_3 at high pressure. Subsequent topological analysis of Bader charges in $(NH_3)_2Xe$ at selected pressures using the quantum theory of atoms in molecules [68] is shown in Table S2 in the SM [58]. At 11 GPa, two N atoms gain 2.33 electrons—2.29 from H atoms and 0.04 from Xe atoms—indicating weakly ionic interaction between Xe and N atoms. This is like interactions in H_2O-He [1,2,69], He-N_4 [4], NH_3-He [5,6,69], and FeO_2He [70] systems, in which only 0.02–0.07 of an electron is donated by each He atom. Surprisingly, the charge transferred to N from Xe increases with increasing pressure; the 0.13 of an electron donated at 200 GPa indicates considerable ionic interaction between Xe and NH_3. The increasing interaction between Xe and NH_3 is further confirmed by Laplacian charge density calculations [71], which show values between Xe and NH_3 increasing from 0 at 11 GPa to 3.05 at 200 GPa, as shown in Table S3 in the SM [58]. We also calculated the distance between the Xe and N atoms in the $(NH_3)_2Xe$ compound as a function of pressure, as shown in Fig. S7 in the SM [58]. The results show that the nearest distances between the Xe and N decrease from ∼2.98 Å at 50 GPa to 2.50 Å at 300 GPa, which induces the stronger interaction between Xe and N atoms. This is consistent with the Bader electron transformation and Laplacian charge density results. The electronic band structures and density of states (DOS) (Fig. S8 in the SM [58]) show that $(NH_3)_2Xe$ is an insulator with wide bandgaps of 5.66 and 5.97 eV at 11 and 80 GPa, respectively. The absence of negative values of phonon dispersions in phonon dispersion calculations confirm the dynamical stability of these $(NH_3)_2Xe$ phases in their stable pressure ranges, as shown in Fig. S9 in the SM [58].

Extensive AIMD calculations and calculated mean squared displacement (MSD) for $(NH_3)_2Xe$ at 11–350 GPa and 100–5000 K clarify its atomic dynamical properties at HPHT. It is generally accepted that diffusion of none, at least one, and all elements in a structure under certain extreme conditions represent solid, superionic, and fluid phases, respectively. The MSD and atomic trajectories of the $P2_12_12_1$ structure at selected conditions (20 GPa@300 K, 20 GPa@500 K, and 34.3 GPa@3500 K) are depicted in Fig. 3. At 300 K and 20 GPa, the $P2_12_12_1$ phase maintains its crystalline configuration with diffusion coefficients of $D^N = D^H = D^{Xe} = 0$, thus predicting $(NH_3)_2Xe$ to be solid at these conditions. As the temperature increases to 500 K, N and Xe continue to vibrate in their lattice positions with $D^N = D^{Xe} = 0$, while the H atom becomes diffusive with a diffusion coefficient of $D^H = 1.48\times10^{-6}$ cm^2 s^{-1} [Fig. 3(b)], which reveals that the predicted $(NH_3)_2Xe$ transforms from a solid to a superionic phase. This character is broken, and a fluid state emerges upon heating to 34.3 GPa@3500 K, and all atoms diffuse ($D^H = 2.21\times10^{-4}$ cm^2 s^{-1}, $D^N = 1.19\times10^{-4}$ cm^2 s^{-1}, and $D^{Xe} = 1.19\times10^{-5}$ cm^2 s^{-1}), as shown in Fig. 3(c). HPHT is needed for $(NH_3)_2Xe$ to form the superionic and fluid phases: for example, 800 K is needed at 103 GPa for the superionic phase and 5200 K for the fluid phase at 124 GPa, as shown in Figs. S10– S12 in the SM [58]. This is reasonable, as the interaction between Xe and NH_3 becomes stronger with increasing

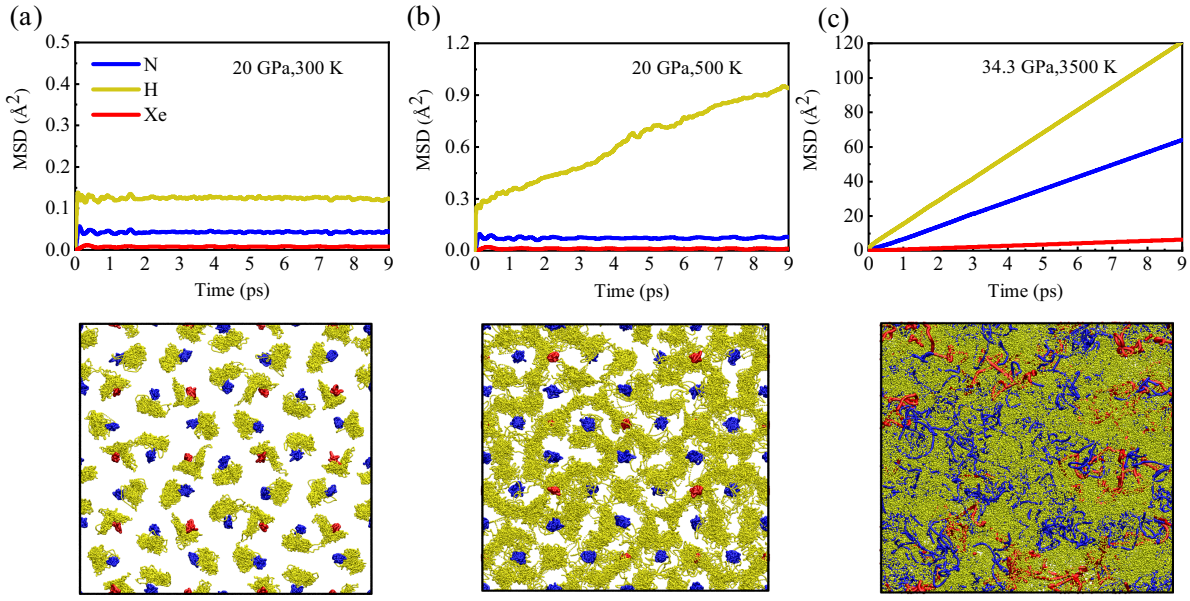

FIG. 3. Calculated mean squared displacement (MSD; upper panel) and atomic trajectories (lower panel) of the atomic positions of the $P2_12_12_1$ structure at (a) 20 GPa and 300 K, (b) 20 GPa and 500 K, and (c) 34.3 GPa and 3500 K.

pressure. We take the $P4_1$ structure as an example to examine the structure change at high temperature at 100 GPa. In the solid state temperature range of 0–500 K, we find that the Xe-N sublattice has only small distortion with slightly changed Xe-N distance and N-Xe-N angle (Fig. S13 in SM [58]). In fact, turning on symmetry for the 500 K simulation leads to the same Xe-N sublattice as in $P4_1$ at 0 K. As the temperature further increases to the superionic region, the distortion of the Xe-N sublattice becomes larger, and the symmetry of the Xe-N sublattice is lowered to $P1$ at 3000 K. The broadened radial distribution functions indicate the larger vibrating amplitude of Xe and N atoms at 3000 K than those at 500 K; however, the similar average Xe-N distance suggests the slight distortion of the Xe-N sublattice at this high temperature (Fig. S14 in the SM [58]). Our further analysis shows that the Xe-N sublattice in the $P2_12_12_1$ structure keeps its $P2_12_12_1$ symmetry at high temperature, which is very similar but different to that in the $P4_1$ phase (Fig. S15 in the SM [58]). This indicates that the $P2_12_12_1$ and $P4_1$ phases will transform into two different superionic phases with the temperature increasing. In addition, the temperature (5200 K at 124 GPa) needed for NH_3-Xe to form the fluid phase is much higher than that (3100 K at 124 GPa) for NH_3-He [5,6]; this is understandable, as Xe interacts more strongly with NH_3 than He does, as deduced from the increase in gained electrons.

Figure 4 shows the phase diagram of $(NH_3)_2Xe$ at HPHT based on the AIMD results. It shows three main phase regions: solid (blue area), superionic (dark yellow area), and fluid (orange area). At low temperatures, the boundary (gray line) between the $P2_12_12_1$ and $P4_1$ phases is determined by the difference in Gibbs free energy calculated within the quasiharmonic approximation. The superionic phase exists over broad ranges of high temperatures: 400–3050 K at 11 GPa and 1000 to >5000 K at 350 GPa, which covers the extreme conditions of the layer outside the core of planets such as Uranus, Neptune, Venus, and Earth. This indicates that the predicted superionic $(NH_3)_2Xe$ might be a possible constituent in the layer outside the core of these planets. The region of fluid $(NH_3)_2Xe$ (orange area) covers the extreme conditions inside Jupiter, suggesting that the fluid state of the predicted compound might be present in the interior of Jupiter. Therefore, these predictions of $(NH_3)_2Xe$ could require models of the

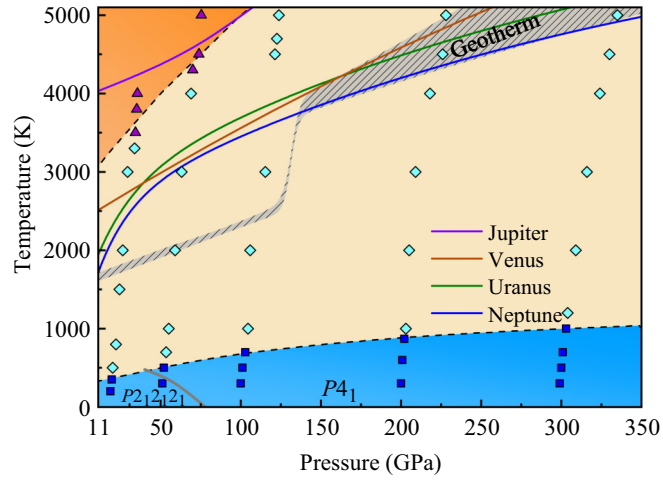

FIG. 4. Phase diagram of $(NH_3)_2Xe$ at high pressures and high temperatures (HPHT) corresponding to planetary interiors. Blue, dark yellow, and orange areas represent solid, superionic, and fluid states, respectively. Plotted points are conditions selected for enhanced *ab initio* molecular dynamics (AIMD) calculations: blue squares, light blue diamonds, and purple triangles represent the solid, superionic, and fluid phases, respectively. The gray line in the blue area indicates the critical transition boundary between the solid $P2_12_12_1$ phase and the $P4_1$ phase. The gray shaded area represents the geothermal energy of the Earth [22], and the blue, green, brown, and purple solid lines represent the isentropic lines of Neptune, Uranus [72], Venus [73], and Jupiter [74], respectively.

interiors of planets to be updated, as Xe could possibly have been trapped in planets during their evolution. The current results also provide important theoretical guidance for further examination of other unconventional stoichiometries of compounds containing C, H, O, and N in the interiors of icy planets [75,76].

IV. CONCLUSIONS

In conclusion, combining structural prediction and first-principles calculations, we systematically investigated the NH_3-Xe system at HPHT. Our prediction shows that >11 GPa, Xe can react with NH_3 to form a stable compound $(NH_3)_2Xe$, which is energetically stable over a broad pressure and temperature window. NH_3 remains molecular in the compound at least to 300 GPa, indicating that the incorporation of Xe could suppress the decomposition of NH_3. Further AIMD calculations reveal that the predicted $(NH_3)_2Xe$ compound exhibits superionic behavior in a region of its phase diagram covering the interior conditions of planets such as Uranus, Neptune, Jupiter, and Venus. These results reveal that the $(NH_3)_2Xe$ compound might be a possible constituent of the layer outside the core of these planets; they also provide essential information for improving the interior models of these planets.

ACKNOWLEDGMENTS

The authors acknowledge funding from the NSFC under Grants No. 12074154, No. 12174160, No. 11804129, No. 11722433, and No. 11804128, and the Science and Technology Project of Xuzhou under Grant No. KC19010. Y.L. acknowledges the funding from the Six Talent Peaks Project and 333 High-level Talents Project of Jiangsu Province. P.Z. acknowledges the founding from Postgraduate Research & Practice Innovation Program of Jiangsu Province No. KYCX20_2217. All calculations were performed at the High-Performance Computing Center of the School of Physics and Electronic Engineering of Jiangsu Normal University.

The authors declare no competing financial interests.

[1] H. Liu, Y. Yao, and D. D. Klug, Phys. Rev. B **91**, 014102 (2015).
[2] C. Liu, H. Gao, Y. Wang, R. J. Needs, C. J. Pickard, J. Sun, H. T. Wang, and D. Xing, Nat. Phys. **15**, 1065 (2019).
[3] X. Dong, A. R. Oganov, A. F. Goncharov, E. Stavrou, S. Lobanov, G. Saleh, G. R. Qian, Q. Zhu, C. Gatti, V. L. Deringer *et al.*, Nat. Chem. **9**, 440 (2017).
[4] Y. Li, X. Feng, H. Liu, J. Hao, S. A. T. Redfern, W. Lei, D. Liu, and Y. Ma, Nat. Commun. **9**, 722 (2018).
[5] J. Shi, W. Cui, J. Hao, M. Xu, X. Wang, and Y. Li, Nat. Commun. **11**, 3164 (2020).
[6] C. Liu, H. Gao, A. Hermann, Y. Wang, M. Miao, C. J. Pickard, R. J. Needs, H.-T. Wang, D. Xing, and J. Sun, Phys. Rev. X **10**, 021007 (2020).
[7] D. Smith, J. Am. Chem. Soc. **85**, 816 (1963).
[8] D. H. Templeton, A. Zalkin, J. Forrester, and S. M. Williamson, J. Am. Chem. Soc. **85**, 817 (1963).
[9] J. L. Huston, M. H. Studier, and E. N. Sloth, Science **143**, 1161 (1964).
[10] H. Selig, H. H. Claassen, C. L. Chernick, J. G. Malm, and J. L. Huston, Science **143**, 1322 (1964).
[11] A. Dewaele, P. Loubeyre, P. Dumas, and M. Mezouar, Phys. Rev. B **86**, 014103 (2012).
[12] A. Dewaele, N. Worth, C. J. Pickard, R. J. Needs, S. Pascarelli, O. Mathon, M. Mezouar, and T. Irifune, Nat. Chem. **8**, 784 (2016).
[13] Q. Zhu, D. Y. Jung, A. R. Oganov, C. W. Glass, C. Gatti, and A. O. Lyakhov, Nat. Chem. **5**, 61 (2013).
[14] A. Hermann and P. Schwerdtfeger, J. Phys. Chem. Lett. **5**, 4336 (2014).
[15] C. Sanloup, H.-K. Mao, and R. J. Hemley, Proc. Natl. Acad. Sci. USA **99**, 25 (2002).
[16] M. Somayazulu, P. Dera, A. F. Goncharov, S. A. Gramsch, P. Liermann, W. Yang, Z. Liu, H.-K. Mao, and R. J. Hemley, Nat. Chem. **2**, 50 (2010).
[17] C. Sanloup, S. A. Bonev, M. Hochlaf, and H. E. Maynard-Casely, Phys. Rev. Lett. **110**, 265501 (2013).
[18] W. B. Hubbard, Science **214**, 145 (1981).
[19] M. Bethkenhagen, E. R. Meyer, S. Hamel, N. Nettelmann, M. French, L. Scheibe, C. Ticknor, L. A. Collins, J. D. Kress, J. J. Fortney *et al.*, Astrophys. J. **848**, 67 (2017).
[20] N. Nettelmann, K. Wang, J. J. Fortney, S. Hamel, S. Yellamilli, M. Bethkenhagen, and R. Redmer, Icarus **275**, 107 (2016).
[21] A. Vorburger, P. Wurz, and H. Waite, Space Sci. Rev. **216**, 57 (2020).
[22] R. O. Pepin and D. Porcelli, Rev. Mineral. Geochem. **47**, 191 (2002).
[23] P. Mahaffy, H. Niemann, A. Alpert, S. Atreya, J. Demick, T. Donahue, D. Harpold, and T. Owen, J. Geophys. Res. **105**, 15061 (2000).
[24] T. M. Donahue, J. H. Hoffman, and R. R. Hodges Jr., Geophys. Res. Lett. **8**, 513 (1981).
[25] K. A. Goettel and J. S. Lewis, J. Atmos. Sci. **31**, 828 (1974).
[26] S. Atreya, P. Mahaffy, H. Niemann, M. Wong, and T. Owen, Planet. Space Sci. **51**, 105 (2003).
[27] R. Wieler, Rev. Mineral. Geochem. **47**, 21 (2002).
[28] Y. Wang, J. Zhang, H. Liu, and G. Yang, Chem. Phys. Lett. **640**, 115 (2015).
[29] D. Li, Y. Liu, F.-B. Tian, S.-L. Wei, Z. Liu, D.-F. Duan, B.-B. Liu, and T. Cui, Front. Phys. **13**, 137107 (2018).
[30] G. Weck, A. Dewaele, and P. Loubeyre, Phys. Rev. B **82**, 014112 (2010).
[31] H. Gao, C. Liu, A. Hermann, R. J. Needs, C. J. Pickard, H. T. Wang, D. Xing, and J. Sun, Natl. Sci. Rev. **7**, 1540 (2020).
[32] L. Zhu, H. Liu, C. J. Pickard, G. Zou, and Y. Ma, Nat. Chem. **6**, 644 (2014).
[33] F. Peng, X. Song, C. Liu, Q. Li, M. Miao, C. Chen, and Y. Ma, Nat. Commun. **11**, 5227 (2020).
[34] C. Sanloup, R. J. Hemley, and H.-K. Mao, Geophys. Res. Lett. **29**, 30-1 (2002).
[35] J.-I. Matsuda and K. Matsubara, Geophys. Res. Lett. **16**, 81 (1989).
[36] A. P. Jephcoat, Nature (London) **393**, 355 (1998).

[37] C. Sanloup, B. C. Schmidt, E. M. C. Perez, A. Jambon, E. Gregoryanz, and M. Mezouar, Science **310**, 1174 (2005).
[38] W. B. Hubbard and J. J. MacFarlane, J. Geophys. Res. **85**, 225 (1980).
[39] Y. Wang, J. Lv, L. Zhu, and Y. Ma, Phys. Rev. B **82**, 094116 (2010).
[40] Y. Wang, J. Lv, L. Zhu, and Y. Ma, Comput. Phys. Commun. **183**, 2063 (2012).
[41] B. Gao, P. Gao, S. Lu, J. Lv, Y. Wang, and Y. Ma, Sci. Bull. **64**, 301 (2019).
[42] Y. Li, J. Hao, H. Liu, Y. Li, and Y. Ma, J. Chem. Phys. **140**, 174712 (2014).
[43] Y. Li, J. Hao, H. Liu, S. Lu, and J. S. Tse, Phys. Rev. Lett. **115**, 105502 (2015).
[44] Y. Li, L. Wang, H. Liu, Y. Zhang, J. Hao, C. J. Pickard, J. R. Nelson, R. J. Needs, W. Li, Y. Huang *et al.*, Phys. Rev. B **93**, 020103(R) (2016).
[45] W. Cui and Y. Li, Chin. Phys. B **28**, 107104 (2019).
[46] W. Cui, T. Bi, J. Shi, Y. Li, H. Liu, E. Zurek, and R. J. Hemley, Phys. Rev. B **101**, 134504 (2020).
[47] M. Xu, C. Huang, Y. Li, S. Liu, X. Zhong, P. Jena, E. Kan, and Y. Wang, Phys. Rev. Lett. **124**, 067602 (2020).
[48] B. Liu, W. Cui, J. Shi, L. Zhu, J. Chen, S. Lin, R. Su, J. Ma, K. Yang, M. Xu *et al.*, Phys. Rev. B **98**, 174101 (2018).
[49] J. Chen, W. Cui, K. Gao, J. Hao, J. Shi, and Y. Li, Phys. Rev. Research **2**, 043435 (2020).
[50] S. Ding, J. Shi, J. Xie, W. Cui, P. Zhang, K. Yang, J. Hao, L. Zhang, and Y. Li, npj Comput. Mater. **7**, 89 (2021).
[51] K. Gao, W. Cui, J. Chen, Q. Wang, J. Hao, J. Shi, C. Liu, S. Botti, M. A. L. Marques, and Y. Li, Phys. Rev. B **104**, 214511 (2021).
[52] G. Kresse and J. Furthmüller, Phys. Rev. B **54**, 11169 (1996).
[53] G. Kresse and J. Furthmüller, Comput. Mater. Sci. **6**, 15 (1996).
[54] J. P. Perdew, J. A. Chevary, S. H. Vosko, K. A. Jackson, M. R. Pederson, D. J. Singh, and C. Fiolhais, Phys. Rev. B **46**, 6671 (1992).
[55] J. P. Perdew, K. Burke, and M. Ernzerhof, Phys. Rev. Lett. **77**, 3865 (1996).
[56] G. Kresse and D. Joubert, Phys. Rev. B **59**, 1758 (1999).
[57] W. G. Hoover, Phys. Rev. A **31**, 1695 (1985).
[58] See Supplemental Material at http://link.aps.org/supplemental/10.1103/PhysRevB.105.214109 for crystal structures, energy differences, structural parameters, ELFs, Bader charge character, phonon dispersions, band structures, DOS, MSDs, atomic trajectories, and radial distribution functions.
[59] K. Momma and F. Izumi, J. Appl. Cryst. **44**, 1272 (2011).
[60] S. Grimme, S. Ehrlich, and L. Goerigk, J. Comput. Chem. **32**, 1456 (2011).
[61] T. Bučko, S. Lebegue, J. Hafner, and J. G. Angyan, J. Chem. Theory Comput. **9**, 4293 (2013).
[62] C. J. Pickard and R. Needs, Nat. Mater. **7**, 775 (2008).
[63] T. Palasyuk, I. Troyan, M. Eremets, V. Drozd, S. Medvedev, P. Zaleski-Ejgierd, E. Magos-Palasyuk, H. Wang, S. A. Bonev, D. Dudenko *et al.*, Nat. Commun. **5**, 3460 (2014).
[64] E. Kim, M. Nicol, H. Cynn, and C. S. Yoo, Phys. Rev. Lett. **96**, 035504 (2006).
[65] Y. Li, G. Gao, Q. Li, Y. Ma, and G. Zou, Phys. Rev. B **82**, 064104 (2010).
[66] J. Sun, A. Ruzsinszky, and J. P. Perdew, Phys. Rev. Lett. **115**, 036402 (2015).
[67] J. Sun, R. C. Remsing, Y. Zhang, Z. Sun, A. Ruzsinszky, H. Peng, Z. Yang, A. Paul, U. Waghmare, X. Wu *et al.*, Nat. Chem. **8**, 831 (2016).
[68] R. F. W. Bader, *Atoms in Molecules: A Quantum Theory* Vol. 22 (Clarendon Press, Oxford, UK, 1990).
[69] Y. Bai, Z. Liu, J. Botana, D. Yan, H. Q. Lin, J. Sun, C. J. Pickard, R. J. Needs, and M. S. Miao, Commun. Chem. **2**, 102 (2019).
[70] J. Zhang, J. Lv, H. Li, X. Feng, C. Lu, S. A. T. Redfern, H. Liu, C. Chen, and Y. Ma, Phys. Rev. Lett. **121**, 255703 (2018).
[71] R. F. Bader, Acc. Chem. Res. **18**, 9 (1985).
[72] R. Redmer, T. R. Mattsson, N. Nettelmann, and M. French, Icarus **211**, 798 (2011).
[73] A. Aitta, Icarus **218**, 967 (2012).
[74] W. B. Hubbard and B. Militzer, Astrophys. J. **820**, 80 (2016).
[75] A. S. Naumova, S. V. Lepeshkin, P. V. Bushlanov, and A. R. Oganov, J. Phys. Chem. A **125**, 3936 (2021).
[76] L. J. Conway, C. J. Pickard, and A. Hermann, Proc. Natl. Acad. Sci. USA **118**, e2026360118 (2021).